Document downloaded from:

http://hdl.handle.net/10251/49046

This paper must be cited as:

Blasco-Tamarit, E.; García-García, D.; García Antón, J. (2011). Imposed potential measurement to evaluate the pitting corrosion resistance and the galvanic behaviour of a highly alloyed austenitic stainless steel and its weldment in a LiBr solution at temperatures up to 150ºC. Corrosion Science. 53:784-795.

The final publication is available at

Copyright Elsevier

*Manuscript (revised)
Click here to view linked References

IMPOSED POTENTIAL MEASUREMENTS TO EVALUATE THE PITTING CORROSION RESISTANCE AND THE GALVANIC BEHAVIOUR OF A HIGHLY ALLOYED AUSTENITIC STAINLESS STEEL AND ITS WELDMENT IN A LiBr SOLUTION AT TEMPERATURES UP TO 150 ºC

Blasco-Tamarit, E.; García-García, D.M..; García Antón, J.*;

Ingeniería Electroquímica y Corrosión (IEC). Departamento de Ingeniería Química y Nuclear. E.T.S.I.Industriales.

Universidad Politécnica de Valencia. P.O. Box 22012, E-46071 Valencia. Spain.

ABSTRACT

Pitting corrosion resistance and galvanic behaviour of Alloy 31, a highly alloyed austenitic stainless steel (UNS N08031), and its weldment were studied in a heavy brine LiBr solution 1080 g/l at different temperatures (75 ºC - 150 ºC) using electrochemical techniques. The Mixed Potential Theory was used to evaluate the galvanic corrosion between the base and welded metals. Cyclic potentiodynamic curves indicate that high temperatures make passivation and repassivation of pits difficult, because the whole passivation range and the repassivation potential values decrease with temperature. The Critical Pitting Transition occurs between 100 ºC and 125 ºC.

Keywords: A. Stainless Steels, C. Passivity, C. Welding

1. INTRODUCTION

Lithium Bromide absorption machines are an alternative to refrigeration compression systems, since the refrigerants traditionally used in compression systems were banned in the Montreal Protocol (1987) because they belonged to the chlorofluorocarbon (CFC) group, and their substitutes are submitted to severe regulations (Kyoto Protocol (1997)). Absorption machines use water as refrigerant and Lithium Bromide heavy brine solutions as absorbent, both zero ozone depletion potential fluids and zero global warming potential fluids, that is why absorption technology appears to be a promising alternative to vapour-compression systems [1]. The first absorption machines were single-effect (SE) systems with five main elements: Evaporator, absorber, condenser, generator and heat exchanger. The most aggressive conditions in these systems were 100 ºC and 992 g/l LiBr [2]. Afterwards, double-effect (DE) absorption machines with two generators and two heat exchangers were developed to increase the energy efficiency of single-effect systems; however higher temperatures (up to 170 ºC) and LiBr concentrations (up to 1080 g/l LiBr) are reached in these systems [1]. DE machines generate an additional cooling effect compared to SE and have been used as an industrial standard for a high performance heat-operated refrigeration cycles, but the severe working conditions can aggravate the corrosion problems of the construction materials [3, 4].

The cheapest and first structural material candidate for the construction of structural elements of these machines was carbon steel, however, it is not the most corrosion resistant in many environments [5-8]. For this reason, the most widely used structural materials for this application are 300 series baseline stainless steels (AISI 304, AISI

316, AISI 316L, etc.). There are several references of other authors referred to corrosion caused by LiBr solutions in these materials applied to absorption refrigeration systems [8-13].

The severe conditions of LiBr concentration and temperature reached in the heat zones of DE machines aggravate the corrosion problems on metallic components of these systems; these problems are even more important on the weldments due to the galvanic effect between the base and welded metal, and demand for higher corrosion resistant materials. One method to solve these corrosion problems in double-effect LiBr absorption machines is to use high corrosion-resistant and technologically efficient performance steel tubes [11, 14, 15] in their construction. The development of corrosion-resistant metallic materials, like highly alloyed austenitic stainless steels with large amounts of chromium, nickel and molybdenum (superaustenitic stainless steels), has become one of the key issues in new absorption systems. One of these alloys is Alloy 31 (UNS N08031), with 26.75% Cr, 31.85% Ni and 6.6% Mo. Alloy 31 is an iron-nickel-chromium-molybdenum alloy with nitrogen addition which fills the gap between the existing baseline stainless steels and the nickel alloys, showing greater corrosion resistance than conventional stainless steels and very close to that of the nickel base alloys. Alloy 31 is characterised by its high resistance to corrosion in halide media, yet it can undergo localised preferential pitting corrosion in bromide environments.

In previous works, the authors studied the corrosion behaviour of different materials, especially, copper and copper alloys [16-28], austenitic and duplex stainless steel [14,

15, 27-47], titanium[19, 29, 30, 48, 49] etc. (including their weldments in some studies) in LiBr solutions under different conditions (static, cavitation and flowing conditions) and at temperatures from 25 ºC to 100 ºC and LiBr concentrations from 400 g/l to 992 g/l. In the present study 150 ºC and 1080 g/l LiBr conditions have been reached to reproduce more accurately the real operation conditions in the most problematical zones of double-effect machines. The results of these previous works, in particular those about conventional stainless steels, indicate that all materials passivate in heavy brine LiBr solutions, but their corrosion rates and susceptibility to pitting corrosion increase with temperature and LiBr concentrations. These results can not be directly extrapolated to more aggressive conditions (the decrease in corrosion resistance with temperature could not be linear, as observed in the present study), which implies to carry out tests approaching to the real operation conditions.

The aim of the present work was to study the pitting corrosion resistance and repassivation behaviour of Alloy 31 and welded Alloy 31, as well as their galvanic coupling, in a 1080 g/l heavy brine LiBr solution at 75 ºC, 100 ºC, 125 ºC and 150 ºC.

2. EXPERIMENTAL

The materials tested were the highly-alloyed Austenitic Stainless Steel Alloy 31 (UNS N08031) used as base metal and the welded metal obtained by means of the Gas Tungsten Arc Welding (GTAW) technique using the nickel-base alloy (UNS N06059) as filler metal. Alloy 31 and the filler metal were provided by KRUPP VDM Gmbh. Material compositions are shown in **Table 1**. The working electrodes were cylindrically

shaped and covered with polytetrafluoroethylene (PTFE) coating. To avoid the effect of the cathode/anode area ratio in the galvanic study, the Alloy 31 and welded metal probes were identical (55 mm high and 8 mm in diameter with a 2 mm teflon coating), thus an area of 0.5 cm^2 was exposed to the solution. All the electrodes were wet abraded from 500 SiC (silicon carbide) grit to 4000 SiC grit, and finally rinsed with distilled water.

The welded samples were obtained from the Alloy 31 probes, which had a gap (2.5 mm wide and 3 mm deep) in the upper part of the bar. That gap was filled with the filler metal using the GTAW technique. Welding was applied using a tungsten electrode in an argon atmosphere and the welding conditions were maintained constant in all the welded samples (current 63 A, voltage 14 V and argon flow 10 l/min).

Electrochemical measurements of Alloy 31 and Welded Alloy 31 were achieved in a heavy brine 1080 g/l (12.44 M) LiBr solution prepared from purissimum LiBr (98 %wt). The tests were carried out at 75 ºC, 100 ºC, 125 ºC and 150 ºC in order to study the influence of temperature on Alloy 31 and welded Alloy 31 corrosion resistance. These temperatures were reached using a heater belt located around a horizontal electrochemical cell [50]. All temperatures were below the boiling temperature of the 1080 g/l LiBr solution, i.e. 165 ºC. The heavy brine 1080 g/l LiBr solution was stored at 60 ºC to avoid LiBr crystallisation.

Cyclic potentiodynamic polarisation curves of Alloy 31 and welded Alloy 31 were determined. The potentials of the working electrode were measured vs an external

silver-silver chloride reference electrode with 3M potassium chloride solution. The auxiliary electrode was a platinum wire. Polarisation curves were recorded in LiBr solution deareated for 20 minutes by bubbling nitrogen prior to immersion. A nitrogen atmosphere was maintained over the liquid surface during the whole test to avoid the presence of oxygen, reproducing the real operation conditions of absorption machines. These machines must operate under vacuum conditions, since the presence of gases would reduce the performance of both the condenser and the absorber [3, 51]. Before each polarisation, the sample was immersed in the test solution for 1 h at the Open Circuit Potential (OCP). Cyclic potentiodynamic polarisation curves were then recorded from 150 $mV_{Ag/AgCl}$ below the corrosion potential at 0.5 mV/s sweep rate. When the current density reached 10 mA/cm^2, the potential scan was reversed in order to evaluate the repassivation tendency of the metal. All tests were repeated at least three times in order to verify reproducibility. Corrosion potential (E_{corr}) and corrosion current density (i_{corr}) were estimated to obtain information about the general electrochemical behaviour of the material. Pitting corrosion susceptibility and repassivation behaviour were evaluated from parameters such as pitting potential (E_p), passivation current density (i_p), repassivation potential (E_{rp}) and repassivation current density (i_{rp}). Pitting potentials were reported as the potential at which current density reaches 100 $\mu A/cm^2$ [52]. E_{rp} values were taken at the crossing between the backward and forward scans. Repassivation current density represents the maximum current reached [53].

The galvanic corrosion between the welded and base material was evaluated from the polarisation curves by superimposing the potentiodynamic curves of both alloys. The

galvanic current density and mixed potential of the pairs were estimated from the intersection point, according to the Mixed Potential Theory [54].

3. RESULTS AND DISCUSSION

3.1. OPEN CIRCUIT POTENTIAL

The open circuit potential values of Alloy 31 and welded Alloy 31 in the 1080 g/l LiBr solution at high temperatures are shown in **Table 2**. The OCP values of Alloy 31 shifted to more positive values as temperature increased, increasing around 5 mV/ºC from 100 ºC to 125 ºC. This increase is more than two times the increase rate from 75 ºC to 100 ºC and from 125 ºC to 150 ºC. This ennoblement of the metal with temperature, also reported previously in LiBr medium [40, 44, 55], is due to the fact that although temperature favours the kinetics of corrosion reactions [15, 56-58], it also promotes the fast growth of passive films on metallic surfaces [14, 59-61]. The same tendency with temperature was observed from 100ºC in the welded Alloy 31.

There is a general trend in the open circuit potentials of both materials at the temperatures studied to increase with time at the beginning of the tests and to stabilise at the end of the tests, indicating the ennoblement of the materials and the spontaneous formation of the oxide layer on the metal surface. This behaviour could be attributable to the healing of the pre-immersion air formed oxide film and further thickening of the oxide film as a result of the interaction between the electrolyte and the metal surface [62]. The growth of the oxide film continues until the film reaches a thickness that is stable in the electrolyte. In this case, during the open circuit potential test a passive film

containing Cr_2O_3 (Alloy 31 contains 26.75 % chromium, and consequently welded Alloy 31 too) grows on the electrode surface, shifting the open circuit potentials to higher potentials [63] until they stabilise.

3.2. CYCLIC POTENTIODYNAMIC TESTS

Cyclic potentiodynamic curves of Alloy 31 and welded Alloy 31 in the 1080 g/l LiBr solution were obtained at 75 ºC, 100 ºC, 125 ºC and 175 ºC (**Figure 1**) to study the influence of temperature on the corrosion behaviour of both metals. These polarisation curves can be divided into several potential domains. The *cathodic domain* includes potentials below the corrosion potential, where current density is determined by the the cathodic reaction. **Figure 1** shows a continuous increase in the current density of the cathodic branch as the potential decreases, shifting these cathodic branches to higher current densities as temperature increases. This fact was also observed in previous works in LiBr media as follows: Cyclic potentiodynamic curves of AISI 304 stainless steel [28] and Alloy 31 [40] in 850 g/l LiBr solutions at different temperatures show an increase in the cathodic current densities to higher values with temperature. The same behaviour was observed from the cyclic potentiodynamic curves of a duplex stainless steel in 992 g/l LiBr solutions at different temperatures [44]. This behaviour could be expected if the cathodic reaction were controlled by diffusion, at least partially since a limiting current density is not observed. Temperature enhances the transport of the products to or from the metallic surface, increasing the cathodic reaction rate [28, 64], which favours the cathodic reaction that occurs on the metal surface.

The next potential domain corresponds to the *cathodic-anodic transition*. This domain is characterised by the corrosion potential and the corrosion current density, which will be described in section *3.2.1. Corrosion potential and corrosion current density.*

The third domain corresponds to the *passive plateau*. In this domain the current density of both materials was stable after the corrosion potential and during a wide range of potentials at the temperatures studied, even at 150 ºC, indicating that these curves are typical of a passive material at all temperatures. Moreover, the absence of current density transients along the passive zone at the temperatures studied indicates a lack of metastable pitting and high stability of the passive film even at 150 ºC.

Figure 1 shows a current density peak on the passive zone of the cyclic curves of both metals at the lowest temperatures. Alloy 31 registered these current density peaks at 350 $mV_{Ag/AgCl}$ and 340 $mV_{Ag/AgCl}$ at 75 ºC and 100 ºC respectively, while welded Alloy 31 at 360 $mV_{Ag/AgCl}$ at 75 ºC. In other words, all of them appeared around 350 $mV_{Ag/AgCl}$ wherever this potential was reached. The peak that occurs before the increase in current density due to pitting can be related to the transpassive dissolution of Cr-containing species. This transpassive dissolution of the alloying elements is closely related to the passive film breakdown and localised corrosion phenomena. The result is a depletion of the alloying elements such as Cr in the first atomic layers near the solution, which are the most susceptible to localised attack by aggressive anions [65]. This issue, as described below in the text, is related to the different pitting mechanisms depending on temperature. The initiation of pitting at lower temperatures is related to the transpassive dissolution of the alloying elements (as illustrated by the current density peaks at 75 ºC

and 100 ºC before the onset of pitting in **Figure 1**), while conventional stable pitting occurs at lower potentials [66], when temperature increases to 125 ºC and 150 ºC.

The last domain was characterised by a sharp increase in current density indicative of the *breakdown of the passive film*, which shifted in both materials to more negative potentials as temperature increased. **Figure 1 (a)** highlights that this shift was of more than 300 $mV_{Ag/AgCl}$ as temperature increased from 100 ºC to 125 ºC in Alloy 31, while it was of around 130 $mV_{Ag/AgCl}$ as temperature increased from 75 ºC to 100 ºC and scarcely of 40 $mV_{Ag/AgCl}$ from 125 ºC to 150 ºC. Welded Alloy 31 (**Figure 1 (b)**), the behaviour observed was practically the same. This significant shift of the increase in current density observed between 100 ºC and 125 ºC indicates that the transition from one mode of pitting mechanism to another occurs within this range of temperatures, as it has been commented previously and will be demonstrated with the pitting and repassivation parameters.

Alloy 31 and welded Alloy 31 registered hysteresis loops in the cyclic curves at the temperatures studied, which are characteristic of passivation breakdown on the forward sweep and subsequent repassivation on the backward sweep. This fact means that both materials were able to repassivate after the breakdown of the passive film even at such high temperatures as 150 ºC.

Figure 2 shows images of Alloy 31 and welded Alloy 31 corresponding to the end of the cyclic tests. These images are mosaics created from images obtained with an optical microscope. At temperatures from 75 ºC to 125 ºC the damaged area produced as a

result of corrosion is clearly visible, while the rest of the surface remains metallic. However, at 150 ºC practically the whole surface appears corroded. Qualitatively, **Figure 2** shows how the damaged area increases as temperature increases in both materials. Quantitatively, the percentages of the corroded area with regard to the total electrode area were obtained by means of image analysis techniques using Visilog 6.3 software. Results are shown in **Figure 3.** These values evidence the enlargement of the corroded area with temperature.

Figure 4 shows images of the electrode surfaces where it is possible to observe that the severity of the attack increases with temperature. Bigger pits appeared distributed in the austenite grains of Alloy 31 as temperature increases and the typical dendrites of the welded metal seem to be more noticeable as temperature increases.

3.2.1. Corrosion potential and corrosion current density

Corrosion potential and corrosion current density values (**Figure 5**) were obtained from the cyclic curves in the heavy brine 1080 g/l LiBr solution at different high temperatures **(Figure 1**).

Corrosion potentials of Alloy 31 followed the same tendency as its OCP values, i.e. they shifted towards more positive values with temperature (**Figure 5 (a)**), the greatest increase occurring from 100 ºC to 125 ºC, when E_{corr} increased 4 mV/ºC. This shift of the corrosion potentials to more positive values with temperature was observed in previous works [28, 40, 44] and it seems to be related with the enhancement of the

cathodic reaction with temperature [28], since the displacement of the cathodic branch of the polarisation curves to higher values of current density shifts the corrosion potential to higher values. Similarly, the general tendency of the E_{corr} values was also to increase with temperature in welded Alloy 31.

The corrosion potentials obtained from the potentiodynamic curves were lower than the OCP values, which was due to the polarisation applied during the potentiodynamic sweep [28, 67, 68]. During the open circuit measurements a protective oxide film was formed on the metal surface, shifting the potential to more positive values. However, at the beginning of the potentiodynamic sweep the potential diminished to -1 $V_{Ag/AgCl}$. At this negative potential the metal surface was modified, and the corresponding E_{corr} calculated from the potentiodynamic curve was more negative than the potential obtained under open circuit conditions (OCP value).

The corrosion current densities of both materials were similar up to 100 ºC, but differed at higher temperatures (**Figure 5 (b)**). Corrosion current densities of Alloy 31 increased with temperature from 8.7 $\mu A/cm^2$ at 75 ºC to 62.2 $\mu A/cm^2$ at 150 ºC (**Figure 5 (b)**), the most abrupt increase again occurring from 100 ºC to 125 ºC (1.12 $\mu A/cm^{2}\cdot ºC$). This increase was more than two times higher than those registered between 75 ºC-100 ºC and 125 ºC-150 ºC. Current density increase was even more dramatic in welded Alloy 31, which reached a value of 134 $\mu A/cm^2$ at 150 ºC, i.e. more than fifteen times higher than that obtained at 75 ºC (8.7 $\mu A/cm^2$). In this case the most abrupt increase was from 125 ºC to 150 ºC (4.3 $\mu A/cm^{2}\cdot ºC$). The results demonstrated that the general corrosion

resistance of both Alloy 31 and welded Alloy 31 decreased with temperature since their corrosion rates increase with temperature [28, 40, 57, 58].

3.2.2. Pitting parameters

The pitting corrosion resistance of a passive metal is determined by its susceptibility to local breakdown and initiation of pits. The mechanisms of pitting corrosion have been widely studied in the literature [52, 57, 69-75], as well as, the aggressiveness of bromides to promote the pitting of stainless steels [52, 64, 76-79]. In this work, pitting potentials were measured potentiodynamically at a scan rate of 0.5 mV/s and reported as the potential at which the current density reached 100 $\mu A/cm^2$. Passivation current densities were also obtained from the cyclic potentiodynamic curves as the value of current density that remains stable as potential increases after the corrosion potential. Pitting potentials and passivation current densities of Alloy 31 and welded Alloy 31 in the 1080 g/l LiBr solution at 75 ºC, 100 ºC, 125 ºC and 150 ºC are shown in **Figure 6**. According to the literature, the pitting potential represents the potential limit above with the formation of pitting begins [56]. The more positive the value of pitting potential the more resistant the metal is to pit initiation and the longer the time required for pit initiation at potentials below E_p (but above E_{rp}) [14, 80]. **Figure 6 (a)** shows that the pitting potential of both materials decreases with temperature [28, 40, 44, 58, 81]; this fact indicates a reduction in the pitting corrosion resistance of both metals with temperature.

The greatest decrease in the pitting potentials of both materials was observed between 100 ºC and 125 ºC. Alloy 31 registered a decrease in pitting potential of 13.5 mV/ºC in this range of temperatures, while the decrease from 75 ºC to 100 ºC was much less significant, 5.8 mV/ºC. Finally, the pitting potentials scarcely diminished 1.2 mV/ºC from 125 ºC to 150 ºC. In the case of welded Alloy 31 E_p diminished almost 6 mV/ºC from 100 ºC to 125 ºC, more than two times the decrease from 75 ºC to 100 ºC (2.45 mV/ºC). Also in this material pitting potentials practically coincided at 125 ºC and 150 ºC. Therefore, the effect of temperature on the pitting potential of both materials was almost the same. On the other hand, Alloy 31 registered E_p values higher than those of welded Alloy 31 at the lowest temperatures (75 ºC and 100 ºC), but this behaviour changed at 125 ºC and 150 ºC.

The sharp drop of pitting potentials observed in **Figure 6 (a)** between 100 ºC and 125 ºC indicates the Critical Pitting Temperature (CPT) transition from the transpassive region to stable pitting corrosion. The Critical Pitting Temperature (CPT), which is the lowest temperature at which the growth of stable pits is possible [66], is defined as the temperature at which E_p drops sharply in a plot of the pitting potentials against temperature [58, 62, 66, 81]. However, this drop must occur in a narrow range of temperatures, narrower than the 25 ºC range observed in this paper (between 100 ºC and 125 ºC). Hence, in this study it only can be established the CPT transition, which occurs between 100 ºC and 125 ºC, being the CPT within this range of temperatures. This high CPT value is related to the elevated PRE value of Alloy 31. Laycock, N.J. [82] reported that the molybdenum content is the most important factor in determining the CPT of a given alloy and the effect of other elements can also be included to produce an

empirical pitting resistance equivalent (PRE). According to Laycock, different authors have quoted different equations for the PRE (e.g., PRE = Cr (wt %) + 3.3 Mo (wt %) + 30 N (wt %)) but the CPT in all cases increases linearly with increasing PRE. According to this equation, the PRE value of Alloy 31 is 54.32, a very high value compared with the PRE values of the 300 series baseline steels (PRE (304SS) ≈ 18, PRE (316SS) ≈ 25, PRE (316LSS) ≈ 25), which is in agreement with the high values of CPT obtained in this work.

For a given alloy in a particular test environment, stable conventional pitting does not occur below the CPT and the breakdown observed at high anodic potentials is caused instead by transpassive dissolution before the onset of pitting. But if the CPT is exceeded, then conventional stable pitting can occur and breakdown potentials sharply drop to several hundred millivolts below those required for transpassivity [66]. As observed in **Figure 6 (a)**, the breakdown of the passive film produced by transpassivity occurs at temperatures lower than 100 ºC and at potentials higher than 300 mV, while stable pitting occurs at temperatures higher than 125 ºC and at potentials lower than 150 mV.

As it has been commented, below CPT stable pitting does not occur, at least not before the onset of transpassive corrosion [81]. Transpassive oxidation of a metal implies the formation of species in a valence state higher than that in the primary passive film formed on the alloy. In most cases, these species have much greater solubility and are abstracted in the solution, resulting in the transpassive dissolution of the material, which is more susceptible to localised attack by aggressive anions [65, 83], such as bromides.

In this study, results show that once the transpassive dissolution happens, the high bromide concentration leads to the pitting of the alloy.

Results have demonstrated that temperature favours pitting on the alloys, which is due to the fact that in general temperature favours the kinetic reactions, and more specifically, the anodic dissolution of the metal in the active zone located inside the cavity. This anodic dissolution of the metal contributes with metallic cations inside the pit. The hydrolysis of these metallic ions reduces the local pH, and the electroneutrality produces the migration of Br^- into the pit [74, 75, 84, 85], making the local conditions more aggressive, so that the metal dissolution continues. Moreover, according to some authors [86-90], the release of aggressive anions from pits and the diffusion over the electrode surface causes weakening of the protective passive film and each active pit increases the probability of creation of further pits in its vicinity.

During the passivation range, the corrosion rate of Alloy 31 and welded Alloy 31 was determined by its passivation current densities (**Figure 6 (b)**). This figure shows that the values registered by Alloy 31 and welded Alloy 31 increased with temperature following an almost linear trend during the whole range of temperatures with a similar increase rate, 0.5 $\mu A/cm^2/^oC$ and 0.7 $\mu A/cm^2/^oC$ respectively. Welded Alloy 31 registered higher values of passivation current densities than the base metal at the temperatures studied.

Passivation current densities were not lower than their corresponding corrosion current densities, although both materials presented stable passivation ranges without pitting

under all the studied conditions due to the formation of the passive film. It is generally accepted that Cr_2O_3-based products form these barrier layers that are responsible for the superior corrosion resistance of stainless steels [59, 91]. These passive films consist of two regions, an inner zone essentially formed of chromium oxide (Cr_2O_3) whose composition is practically constant, and an outer region mainly composed of a mixture of iron and nickel oxides, whose composition depends on external parameters [61, 92]. Although oxides of chromium are the main components of the passive films, S. Ramya [93] also detected the presence of other species as nitrates formed due to the nitrogen content of the alloy (0.193 % N in the case of Alloy 31), by means of Laser Raman microscopic studies of passive films formed on austenitic stainless steels in chloride media. In LiBr media, after the passive film is formed, bromide ions can be adsorbed on the film and replace the oxygen position in the film, forming a soluble metal bromide, destroying the film and increasing corrosion rates [14]. This is in relation to passivation, but when highly alloyed stainless steels reach the transpassive potentials at temperatures lower than the CPT, transpassive dissolution of the chromium, molybdenum and to a lesser extent the nickel that were on the the passive film occurs [83]. Transpassive oxidation is a complex process including the growth of a passive film via generation, transport and consumption of ionic defects, continuous changes in the stoichiometry of the first atomic layers of the film adjacent to the electrolyte, charge transfer reactions at the film/electrolyte interface and transport of reaction products in the bulk solution.

The transition from transpassive corrosion to pitting corrosion upon increasing the temperature indicates that steel resistance to pitting corrosion depends on the solution

temperature [62]. Results reveals that the pitting corrosion resistance of Alloy 31 and welded Alloy 31 decreases with temperature, since pitting potentials decreased (**Figure 6 (a)**) and passivation current densities increased (**Figure 6 (b)**) with temperature. This fact occurs because the properties of the passive film degraded with temperature, the passive films formed at lower temperatures being significantly less defective and more resistant to film breakdown than those formed at higher temperatures. This same behaviour has been reported by several authors [60, 94, 95]. Generally, dissolution processes can accompany the formation of the passive films in high-temperature aqueous enviroments, which could affect the outer layer of the films while the inner chromium oxide layer would be less affected [96]. In this sense, Hur [60] suggested that important changes in the composition of the films with increasing temperature are responsible for this decrease in the protective properties of the film formed at high temperatures. Wang [94] also reported that when temperature increases the resistance of the passive film to breakdown decreases. They attributed this fact to two reasons: on the one hand, the porosity of the passive film increases with temperature; and, on the other hand, an intrinsic modification of the chemical composition and/or physical structure of the passive film takes place. Manning and Duquette [95] found that the oxide film on stainless steels changes from p-type at room temperature to n-type at higher temperatures.

3.2.3. Repassivation parameters

The parameters related to the repassivation behaviour of Alloy 31 and welded Alloy 31 in the 1080 g/l LiBr solution at 75 ºC, 100 ºC, 125 ºC and 150 ºC are shown in **Figure 7**.

The repassivation potential (E_{rp}) is plotted in **Figure 7 (a)**. This parameter refers to the limit below which the metal remains passive and even active pits repassivate. **Figure 7 (a)** shows that, in general, repassivation potential values shifted to more negative values as temperature increased in both materials, the repassivation potential values of welded Alloy 31 being higher than those of the base metal at the temperatures studied. This decrease of E_{rp} with temperature indicates that pit propagation is increasingly stable as temperature increases, therefore, repassivation of propagating pits becomes more difficult as temperature increases.

Alloy 31 registered the highest decrease of E_{rp} between 100 ºC and 125 ºC (3.5 mV/ºC) (**Figure 7 (a)**), which corresponds to the Critical Protection Temperature (CPrT) transition. Different authors have determined the CPrT from the sharp drop of potentials when E_{rp} is plotted versus temperature [56, 62]. E.A. Abd El Meguid [62] reported that CPrT occurs at a lower temperature level than CPT, indicating that stable pits formed at CPT can grow at lower temperatures. This fact can not be verified in Alloy 31 because the CPT and CPrT values are in the same range of temperatures (100 ºC-125 ºC), but in the case of welded Alloy 31 the CPrT transition was between 75 ºC and 100 ºC (**Figure 7 (a)**), therefore at lower temperatures than the CPT transition.

Figure 7 (b) shows the whole passivation range (E_p-E_{corr}). According to Neville and Hodkies [97], the difference between the pitting potential and the corrosion potential was taken as an indicator of the range of potentials in which the metal was passive (*passivity region*). These values are used as an indication of the tendency to nucleation pitting in the metal [56], the greater the difference the greater the resistance of the

material to pitting corrosion. In general, E_p-E_{corr} values decrease with temperature in both materials (**Figure 7 (b)**), indicating that temperature makes the passivation of both metals difficult in the 1080 g/l LiBr solution, since the whole passivation ranges diminish as temperature increases. Alloy 31 presented wider passivation ranges than the welded metal up to 100 ºC, but this behaviour changed at 125ºC and 150 ºC.

The E_{rp} value can be used to define two passivity regions: the stable (E_{rp}-E_{corr}) and the unstable (E_p-E_{rp}) passivity region [56, 98]. The E_{rp}-E_{corr} difference was defined as the perfect/stable passivity region according to Bellezze et al. [98], where pitting corrosion cannot initiate and, furthermore, existing pits cannot propagate. The imperfect/unstable passivity region was defined by the potential range (E_p-E_{rp}) and corresponds to the region where pits cannot initiate but existing pits can propagate. Intermediate values between E_p and E_{rp} affect the probability for pitting to occur over extended exposure time, with the probability of pit initiation approaching to zero near E_{rp}. This (E_p–E_{rp}) value also defines the anodic hysteresis loop, which reflects the repassivation tendency of pitting since it is a measure of the growth tendency of nucleated pitting. **Figure 7 (c)** shows the anodic hysteresis loop (E_p-E_{rp}) of both materials in the 1080 g/l LiBr solution at the different high temperatures under study. In the case of Alloy 31, (E_p-E_{rp}) values decreases with temperature, but welded Alloy 31 registered a first increase of (E_p-E_{rp}) as temperature increases from 75 ºC to 100 ºC, followed by a decrease up to 125 ºC. The last behaviour was also reported by other authors [62], who attribute this peak in the (E_p-E_{rp}) value to the formation of metastable pits below the CPT that can grow at higher anodic current densities. The highest decrease in the E_p-E_{rp} values of both materials again occurred between 100 ºC and 125 ºC, 7.4 mV/ºC in the case of Alloy 31 and 4.4

mV/ºC in welded Alloy 31, indicating the CPT transition. **Figure 7 (c)** shows that above the CPT, the values of (E_p-E_{rp}) tend to be practically temperature independent. This behaviour was also reported previously [62] and suggests that stable pits have their own pitting solution compositions which are independent of the bulk environment. The differences between the anodic hysteresis loop of Alloy 31 and welded Alloy 31 decreased with temperature, being minimal from 125ºC.

Regarding the repassivation of pits, the narrowing of the hysteresis loop of a potentiodynamic cyclic curve is in general related to a better repassivation capacity [56, 98]. The reasons why the hysteresis loop narrows must be considered, since it should be associated with a shift of the E_{rp} to higher values as indicative of good repassivation properties. In this study the hysteresis loop narrows as temperature increases (**Figure 7 (c)**), but this is due to the fact that E_p decreases much more than E_{rp}, which also diminishes. Therefore, this fact can not be associated witha less difficult repassivation of pits with temperature. In this case, it is necessary to consider the E_{rp} values to establish the repassivation behaviour of the materials, and results demonstrate that repassivation of pits becomes more difficult as temperature increases since E_{rp} decreases with temperature.

Figure 8 shows the passive ranges obtained from the cyclic potentiodynamic curves of Alloy 31 and welded Alloy 31 in the 1080 g/l LiBr solution at different temperatures. The OCP values have been located within the corresponding passive ranges. It can be observed that the OCP values of both materials coincided within their respective passive

range at the temperatures studied, which means that Alloy 31 and welded Alloy 31 spontaneously passivated under the studied conditions

The displacement of the OCP with temperature is more significant in Alloy 31 since the OCP values shifted from the perfect passivity region to the imperfect passivity region as temperature increased, being around the pitting potential at 150 ºC, **Figure 8 (a)**. Regarding welded Alloy 31, **Figure 8 (b)**, the OCP values were located in the perfect passive region at temperatures below the CPT (75 ºC and 100 ºC) and in the imperfect passive region at temperatures above the CPT (125 ºC and 150 ºC). Finally, both materials show similar behaviours, since according to the results, under the open circuit potential condition pitting corrosion will not initiate in the 1080 g/l LiBr solution and, furthermore, existing pits will not propagate below the CPT. However, if pits exist on the surface before immersion (as defects etc.), they propagate above the CPT.

3.2.4. Arrhenius plots

The results above mentioned have demonstrated that temperature caused an increase in the corrosion current density of Alloy 31 and welded Alloy 31 in the 1080 g/l LiBr solution. In general, this increase in the corrosion rate, which is represented by the corrosion current density (i_{corr}), with temperature follows Arrhenius equation (eq.1) [99-101]:

$$\log i_{corr} = \log A - \frac{E_a}{2.303RT} \qquad \text{(Eq.1)}$$

where E_a (J/mol) is the molar activation energy of the process, *R* is the gas constant (8.314 J/mol/K), T is the temperature (K) and A is a constant. The molar activation energy of an electrochemical process refers to the energy level that must be overcome by the electron in the exchange through the electrode/ electrolyte interphase. Arrhenius equation indicates that the faster the dependence of the corrosion rate to temperature the higher the E_a [99].

The Arrhenius plots of the current densities registered at different potentials on the cyclic potentiodynamic curves can be used to evaluate the different effects of temperature in different potential regions [57]. **Figure 9** shows the Arrhenius plot for a cathodic potential (-950 $mV_{Ag/AgCl}$), for the corrosion potential, for a potential in the perfect passive region [56, 98] (-450 $mV_{Ag/AgCl}$ in the case of Alloy 31 and -230 in the case of welded Alloy 31) and for a potential in the imperfect passive region [56, 98] (0 $mV_{Ag/AgCl}$). No differences in the data obtained from tests conducted below or above the CPT transitions at the different potentials are observed in **Figure 9**.

The most abrupt increase in current density with temperature occurred at the cathodic potentials in both materials (**Figure 9**), as the highest slopes reflected, indicating that the most noticeable influence of temperature was on the cathodic reaction in both materials. This fact is related to the shift of the corrosion potentials to higher values as temperature increases. Consequently, the highest values of activation energies correspond to the cathodic processes, 55 kJ/mol and 61 kJ/mol for Alloy 31 and welded Alloy 31 respectively. No big differences between the two materials were observed in terms of the cathodic reaction.

In the case of Alloy 31, very similar values of activation energy were registered at the corrosion potential, in the perfect passive region and in the imperfect one, 33 kJ/mol, 34 kJ/mol, 27 kJ/mol respectively. This fact indicates that the dependence of the current density established during the passivation range with temperature is similar along the whole passive range. Regarding the welded metal, the activation energy diminishes from the corrosion potential (50 kJ/mol), to the perfect passivity region (21 kJ/mol) and the imperfect one (9 kJ/mol). In this case, the dependence of the current density established during the perfect passivity region with temperature is stronger than that established during the imperfect passivity one. That is, the increase in the corrosion rate with temperature is slower as the potential shifts to more positive values.

4. GALVANIC CORROSION

The materials were examined by Scanning Electron Microscopy (SEM) in order to estimate possible microstructural variations produced during the GTAW welding procedure that could explain a different corrosion behaviour of the parts of the galvanic pair. **Figure 10 (a)** shows the microstructure of Alloy 31 after etching [102, 103]. This is a single-phase austenite microstructure with equiaxed grains, characteristic of an iron-nickel-chromium-molybdenum alloy like Alloy 31.

Figure 10 (b) shows the dendritic microstructure of austenite characteristic of solidification of metals. An Energy Dispersive X-Ray analysis (EDX) was used to identify the changes in the welded metal composition. Results obtained from this

analysis are shown in **Figure 11**. This figure shows that the content of chromium and especially molybdenum, diminished in the dendrite cores relative to the bulk but increased in the grain boundaries. Concretely, the dendrite cores presented 3 % chromium and 23 % molybdenum less than the grain boundaries. This fact reflects chromium and molybdenum accumulations in the grain boundaries of welded metal, which increases the dissimilarity between the base and the welded metal.

Table 3 summarizes the corrosion potential (E_{corr}) of Alloy 31 and the welded Alloy 31, as well as the mixed potential (E_{couple}) between the pair and the differences between the corrosion potential of the cathodic and the anodic part of the pair (E_C-E_A). In the same way, **Table 3** shows the corrosion current density (i_{corr}) of the uncoupled metals, the galvanic current density generated due to the coupling of the pair (i_G) and the ratio i_G/i_{corr}. Letters "A" (anodic) and "C" (cathodic) indicate the character of each part in the pair.

The corrosion potential of Alloy 31 was lower than the corrosion potential of welded Alloy 31 in the range of temperatures between 75 ºC and 100 ºC (**Table 3**), indicating that Alloy 31 was the anode of the pair. This fact could be attributed to the higher nickel and molybdenum content of the filler metal (60.58 % and 15.40 % respectively) used to obtain the welded metal with respect to the base metal (31.85 % and 6.60 % respectively) [41, 47]. However, welded Alloy 31 was the anode at the highest temperatures (125 ºC and 150 ºC). The more positive mixed potentials were obtained at the highest temperatures (125 ºC and 150 ºC).

Minimal differences of 100-130 mV between the corrosion potential of the cathodic and the anodic part of the pair (E_C-E_A) are necessary to consider the galvanic effect relevant [64], so that according to this fact the galvanic effect was not significant.

Table 3 shows that the galvanic corrosion between the base and the welded Alloy 31 hardly increases with temperature, reaching the elevated value of 182.5 μA/cm^2 at 150 ºC, a value more than thirty five times higher than that registered at 75 ºC.

The corrosion resistance of the anode decreased due to the galvanic effect produced by coupling between the base and the welded metal, since the galvanic current density was higher than its respective corrosion current density at 100 ºC, 125 ºC and 150 ºC (**Table 3**). This fact does not occur at 75 ºC, although the increase in the corrosion resistance of the anode due to coupling was not significant. According to Mansfeld and Kendel [104], this relative increase in the corrosion rate of the anodic part of the pair could be expressed by the ratio i_G/i_{corr}, where i_G is the galvanic current density and i_{corr} is the corrosion current density of the uncoupled anodic part. The magnitude of this ratio may be used as a guide that reflects the severity of the galvanic effect in a couple, and it was suggested that a value lower than 5 implies compatibility of the parts in the couple [105]. Thus, in spite of the high values of galvanic current density registered by the pair in the 1080 g/l LiBr solution, the low values of the ratio i_G/i_{corr} (all of them lower than 1.4) demonstrated the compatibility of the parts of the pair.

5. CONCLUSIONS

The open circuit potentials of both materials increase with time at the temperatures studied, indicating the ennoblement of the materials and the spontaneous formation of the oxide layer on the metal surface.

Alloy 31 and welded Alloy 31 present potentiodynamic cyclic curves typical of passive alloys at all temperatures. The absence of current density transients along the passive zone at the temperatures studied indicates a lack of metastable pitting and high stability of the passive film even at 150 ºC.

The presence of hysteresis loops in the cyclic curves at the temperatures studied indicates that both materials were able to repassivate after the breakdown of the passive film even at such high temperatures as 150 ºC.

Results demonstrated qualitatively and quantitatively the enlargement of the corroded area with temperature.

Corrosion current densities of materials increased with temperature following the Arrhenius equation. Therefore, results demonstrated that the general corrosion resistance of both Alloy 31 and welded Alloy 31 decreased with temperature.

Based on the criteria used to define the pitting potential and the passivation current density in this paper, the pitting corrosion resistance of Alloy 31 and welded Alloy 31

decreases as temperature increases, since pitting potentials decreased and passivation current densities increased with temperature.

Temperature makes the passivation of both metals difficult in the 1080 g/l LiBr solution, since the whole passivation range diminishes as temperature increases. The repassivation of pits is also more difficult as temperature increases, as demonstrated by the decrease of the repassivation potential values with temperature.

The more dramatic changes in the pitting and repassivation parameters obtained according to the criteria used in this paper, occur between 100 ºC and 125 ºC in both materials, indicating that the CPT transition from transpassive dissolution before the onset of pitting to conventional stable pitting occurs in this range of temperatures.

Results obtained following the methodology described in this paper indicates that Alloy 31 and welded Alloy 31 spontaneously passivated under the studied conditions. Under the open circuit potential condition pitting corrosion will not initiate in the 1080 g/l LiBr solution and, furthermore, existing pits will not propagate below the CPT (75 ºC and 100 ºC). However, if pits exist on the surface before immersion (as defects etc.), they will propagate above the CPT (125 ºC and 150 ºC).

Galvanic corrosion between the base and the welded Alloy 31 hardly increases with temperature. However, in spite of the high values of galvanic current density registered by the pair, the low values of the ratio i_G/i_{corr} demonstrated the compatibility of the parts of the pair at the temperatures studied.

6. ACKNOWLEDGEMENTS

We wish to express our gratitude to Ministerio de Ciencia e Innovación (CTQ2009-07518/PPQ) for its financial support, to Dr. Helena Elves from Krupp VDM for supplying the materials and to Dr. M. Asunción Jaime for her translation assistance.

7. REFERENCES

[1] R. D. Misra, P. K. Sahoo, A. Gupta, Thermoeconomic evaluation and optimization of a double-effect H2O/LiBr vapour-absorption refrigeration system. International Journal of Refrigeration 28 (2005) 331-343.

[2] R. D. Misra, P. K. Sahoo, S. Sahoo, A. Gupta, Thermoeconomic optimization of a single effect water/LiBr vapour absorption refrigeration system. International Journal of Refrigeration 26 (2003) 158-169.

[3] Pongsid Srikhirin, Satha Aphornratana, Supachart Chungpaibulpatana, A review of absorption refrigeration technologies. Renewable and Sustainable Energy Reviews 5 (2001) 343-372.

[4] Shenyi Wu, Ian W.Eames, Innovations in vapour-absorption cycles. Applied Energy (2000) 251-266.

[5] C. H. Liang, X. Q. Hu, L. Ma, Effects of Na3PW12O40 on the corrosion behaviour of carbon steel in 55 %LiBr solution. Materials and Corrosion 58 (2007) 39-43.

[6] E. Sarmiento-Bustos, J. G. González-Rodriguez, J. Uruchurtu, A study of the corrosion inhibition of carbon steel in a bromide solution using fractal analysis. Surface and Coatings Technology 203 (2008) 46-51.

[7] Xianqi Hua, Chenghao Liang, Effect of PWVA/Sb2O3 complex inhibitor on the corrosion behavior of carbon steel in 55%LiBr solution. Materials Chemistry and Physics 110 (2008) 285-290.

[8] E. Sarmiento-Bustos, J. G. González-Rodriguez, J. Uruchurtu, V. M. Salinas-Bravo, Corrosion behavior of iron-based alloys in the LiBr + ethylene glycol + H2O mixture. Corrosion Science 51 (2009) 1107-1114.

[9] D. Itzhak, O. Elias, Behavior of Type 304 and Type 316 Austenitic Stainless Steels in 55% Lithium Bromide Heavy Brine Environments. Corrosion 50 (1994) 131-137.

[10] D. Itzhak, O. Elias, Y. Greenberg, Behavior of Type 316 Austenitic Stainless Steel Under Slow Strain Rate Technique Conditions in Lithium Bromide Heavy Brine Environments. Corrosion 52 (1996) 72-78.

[11] B. Brandt, Corrosion behavior of selected materials in lithium bromide solution for the application absorption chillers. Materials and Corrosion 55 (2004) 536-542.

[12] C. Cuevas-Arteaga, J. Porcayo-Calderón, Electrochemical noise analysis in the frequency domain and determination of corrosion rates for SS-304 stainless steel. Materials Science and Engineering A 435-436 (2006) 439-446.

[13] C. Cuevas-Arteaga, M. O. Concha-Guzmán, Corrosion study of SS-316L exposed to LiBr-H2O solution applying electrochemical techniques and weight loss method. Corrosion, engineering, science and technology 44 (2009) 57-68.

[14] A. Igual-Muñoz, J. García-Antón, J. L. Guiñón, V. Pérez-Herranz, Effects of solution temperature on localized corrosion of high nickel content stainless steels and nickel in chromated LiBr solution. Corrosion Science 48 (2006) 3349-3374.

[15] A. Igual-Muñoz, J. García-Antón, S. López Nuévalos, J. L. Guiñón, V. Pérez-Herranz, Corrosion studies of austenitic and duplex stainless steels in aqueous lithium bromide solution at different temperatures. Corrosion Science 46 (2004) 2955-2974.

[16] A. Igual-Muñoz, J. García-Antón, J. L. Guiñón, V. Pérez-Herranz, Galvanic study of zinc and copper in LiBr solutions at different temperatures . Corrosion 57 (2001) 516.

[17] V. Pérez-Herranz, M. T. Montañés, J. García-Antón, J. L. Guiñón, Effect of fluid velocity and exposure time on copper corrosion in a concentrated lithium bromide solution. Corrosion 57 (2001) 835-842.

[18] A. Igual-Muñoz, J. García-Antón, J. L. Guiñón, V. Pérez-Herranz, Effect of aqueous LiBr solutions on the corrosion resistance and galvanic behaviour of Cu-Ni alloys. Corrosion 59 (2003) 32-41.

[19] A. Igual-Muñoz, J. García-Antón, J. L. Guiñón, V. Pérez-Herranz, Galvanic studies of copper coupled to Alloy 33 and Titanium in LiBr solutions. Corrosion 58 (2002) 995-1003.

[20] M. J. Muñoz-Portero, J. García-Antón, J. L. Guiñón, V. Pérez-Herranz, Pourbaix diagrams for copper in aqueous lithium bromide concentrated solutions. Corrosion 60 (2004) 749.

[21] A. Igual-Muñoz, J. García-Antón, J. L. Guiñón, V. Pérez-Herranz, Comparison of inorganic inhibitors of copper, nickel and copper-nickels in aqueous LiBr solution. Electrochimica Acta 50 (2004) 957-966.

[22] M. J. Muñoz-Portero, J. García-Antón, V. Guiñón-Pina, V. Pérez-Herranz, Comparison of anodic polarization behaviour for copper in aqueous lithium bromide concentrated solutions with Pourbaix diagrams. Corrosion 61 (2005) 464-472.

[23] M. T. Montañés, V. Pérez-Herranz, J. García-Antón, J. L. Guiñón, Evolution with exposure time of copper corrosion in a concentrated lithium bromide solution characterization of corrosion products by EDX-analysis and X-Ray diffraction. Corrosion 62 (2006) 64-73.

[24] A. Valero-Gómez, A. Igual-Muñoz, J. García-Antón, Corrosion and galvanic behavior of copper and copper-brazed joints in heavy brine LiBr solutions. Corrosion 62 (2006) 1117-1131.

[25] A. Valero-Gómez, J. García-Antón, A. Igual-Muñoz, Corrosion behaviour of copper-phosphorus-silver brazing alloys in LiBr solutions. Corrosion 62 (2006) 751-764.

[26] M. J. Muñoz-Portero, J. García-Antón, J. L. Guiñón, V. Pérez-Herranz, Corrosion of copper in aqueous lithium bromide concentrated solutions by immersion testing. Corrosion 62 (2006) 1018-1027.

[27] M. T. Montañés, R. Sánchez-Tovar, J. García-Antón, V. Pérez-Herranz, The influence of Reynolds number on the galvanic corrosion of the copper/AISI 304 pair in aqueous LiBr solutions. Corrosion Science 51 (2009) 2733-2742.

[28] R. Sánchez-Tovar, M. T. Montañés, J. García-Antón, The effect of temperature on the galvanic corrosion of copper/AISI 304 pair in LiBr solutions under hydrodynamic conditions. Corrosion Science 52 (2010) 722-733.

[29] J. L. Guiñón, J. García-Antón, V. Pérez-Herranz, G. Lacoste, Corrosion of Carbon steels, Stainless Steels, and Titanium in Aqueous Lithium Bromide Solution. Corrosion 50 (1994) 240-246.

[30] A. Igual-Muñoz, J. García-Antón, J. L. Guiñón, V. Pérez-Herranz, Corrosion behaviour and galvanic coupling of stainless steels, titanium and Alloy 33 in Lithium Bromide solutions. Corrosion 59 (2003) 606-615.

[31] A. Igual-Muñoz, J. García-Antón, J. L. Guiñón, V. Pérez-Herranz, Corrosion Behavior of Austenitic and Duplex Stainless Steel Weldings in Aqueous Lithium Bromide Solution. Corrosion 60 (2004) 982-995.

[32] A. Igual-Muñoz, J. García-Antón, J. L. Guiñón, V. Pérez-Herranz, Effect of Nitrogen in Argon as a Shielding Gas on Tungsten Inert Gas Welds of Duplex Stainless Steels. Corrosion 61 (2005) 693-705.

[33] E. Blasco-Tamarit, A. Igual-Muñoz, J. García-Antón, D. García-García, Effect of aqueous LiBr solutions on the corrosion resistance and galvanic corrosion of an austenitic stainless steel in its welded and non-welded condition. Corrosion Science 48 (2006) 863-886.

[34] D. M. García-García, A. Igual-Muñoz, J. García-Antón, E. Blasco-Tamarit, Effect of cavitation on the corrosion behaviour of welded and non-welded duplex stainless steel in aqueous LiBr solutions . Corrosion Science 48 (2006) 2380-2405.

[35] A. Igual-Muñoz, J. García-Antón, J. L. Guiñón, V. Pérez-Herranz, The effect of chromate in the corrosion behaviour of duplex stainless steel in LiBr solutions. Corrosion Science 48 (2006) 4127-4151.

[36] A. Igual-Muñoz, J. García-Antón, J. L. Guiñón, V. Pérez-Herranz, Inhibition effect of chromate on the passivation and pitting corrosion of a duplex stainless steel in LiBr solutions using electrochemical techniques. Corrosion Science 49 (2007) 3200-3225.

[37] E. Blasco-Tamarit, A. Igual-Muñoz, J. García-Antón, Galvanic Corrosion of high alloyed austenitic stainless steel welds in LiBr Systems. Corrosion Science 49 (2007) 4452-4471.

[38] E. Blasco-Tamarit, A. Igual-Muñoz, J. García-Antón, Effect of temperature on the galvanic corrosion of a high alloyed austenitic stainless steel in its welded and non-welded condition in LiBr solutions. Corrosion Science 49 (2007) 4472-4490.

[39] D. García-García, J. García-Antón, A. Igual-Muñoz, E. Blasco-Tamarit, Cavitation - Corrosion studies on welded and non-welded duplex stainless steel in aqueous LiBr solutions. Corrosion 63 (2007) 462-479.

[40] E. Blasco-Tamarit, A. Igual-Muñoz, J. García-Antón, D. García-García, Effect of temperature on the corrosion resistance and pitting behaviour of Alloy 31 in LiBr solutions. Corrosion Science 50 (2008) 1848-1857.

[41] E. Blasco-Tamarit, A. Igual-Muñoz, J. García-Antón, D. García-García, Comparison between open circuit and imposed potential measurrements to evaluate the effect of temperature on galvanic corrosion of the pair alloy 31-welded alloy 31 in LiBr solutions. Corrosion Science 50 (2008) 3590-3598.

[42] D. García-García, J. García-Antón, A. Igual-Muñoz, Influence of cavitation on the passive behaviour of duplex stainless steels in aqueous libr solutions. Corrosion Science 50 (2008) 2560-2571.

[43] R. Leiva-García, M. J. Muñoz-Portero, J. García-Antón, Evaluation of Alloy 146, 279, 900, and 926 sensitization to intergranular corrosion by means of electrochemical methods and image analysis. Corrosion Science 51 (2009) 2080-2091.

[44] R. Leiva-García, M. J. Muñoz-Portero, J. García-Antón, Corrosion behaviour of sensitized and unsensitized Allloy 900 (UNS 1.4462) in concentrated aqueous lithium bromide solutions at different temperatures. Corrosion Science 52 (2010) 950-959.

[45] R. M. Fernández-Domene, E. Blasco-Tamarit, D. M. García-García, J. García-Antón, Repassivation of the damage generated by cavitation on UNS N08031 in a LiBr solution by means of electrochemical techniques and Confocal Laser Scanning Microscopy. Corrosion Science 52 (2010) 3453-3464.

[46] R. Leiva-García, J. García-Antón, M. J. Muñoz-Portero, Contribution to the elucidation of corrosion initiation through confocal lasers canning microscopy (CLSM). Corrosion Science 52 (2010) 2133-2142.

[47] R. Sánchez-Tovar, M. T. Montañés, J. García-Antón, Effect of different micro-plasma arc welding (MPAW) processes on the corrosion of AISI 316L SS tubes in LiBr and H3PO4 solutions under flowing conditions . Corrosion Science 52 (2010) 1508-1519.

[48] E. Blasco-Tamarit, A. Igual-Muñoz, J. García-Antón, D. García-García, Corrosion behaviour and galvanic coupling of titanium and welded titanium in LiBr solutions. Corrosion Science 49 (2007) 1000-1026.

[49] E. Blasco-Tamarit, A. Igual-Muñoz, J. García-Antón, D. García-García, Galvanic corrosion of titanium coupled to welded titanium in LiBr solutions at different temperatures. Corrosion Science 51 (2009) 1095-1102.

[50] J. García-Antón, A. Igual-Muñoz, J. L. Guiñón, V. Pérez-Herranz, Spain, P-200002526 (2000).

[51] G. A. Florides, S. A. Kalogirou, S. A. Tassou, L. C. Wrobel, Design and construction of a LiBr–water absorption machine. Energy Conversion and Management 44 (2003) 2483-2508.

[52] M. Kaneko, H. S. Isaacs, Pitting of stainless steel in bromide, chloride and bromide/chloride solutions. Corrosion Science 42 (2000) 67-78.

[53] A. Pardo Gutiérrez del Cid, E. Otero Huerta, M. C. Merino Casals, M. D. López González, M. V. Utrilla Esteban, Estudio de la resistencia a la corrosión localizada del acero inoxidable superaustenítico 24,1Cr22Ni7,1Mo en mezclas que contienen iones cloruro y cloruro-fluoruro. Revista Metalúrgica 37 (2001) 499-508.

[54] C. Wagner, Theoretical Analysis of the Current Density Distribution in Electrolytic Cells. Journal of Electrochemical Society 98 (1951) 116-128.

[55] V. Guiñón-Pina, A. Igual-Muñoz, J. García-Antón, Influence of temperature and applied potential on the electrochemical behaviour of nickel in LiBr solutions by means of electrochemical impedance spectroscopy. Corrosion Science 51 (2009) 2406-2415.

[56] A. Pardo, E. Otero, M. C. Merino, M. D. López, M. V. Utrilla, F. Moreno, Influence of pH and Chloride Concentration on the Pitting and Crevice Corrosion Behavior of High-Alloy Stainless Steels. Corrosion 56 (2000) 411-418.

[57] L. F. Garfias-Mesias, J. M. Sykes, Metastable pitting in 25 Cr duplex stainless steel. Corrosion Science 41 (1999) 959-987.

[58] N. J. Laycock, Effects of Temperature and Thiosulfate on Chloride Pitting of Austenitic Stainless Steels. Corrosion 55 (1999) 590-595.

[59] T. Laitinen, N. Bojinov, I. Betova, K. Mäkelä, T. Saario, The properties of and transport phenomena in oxide films on iron, nickel, chromium and their alloys in aqueous enviroments. STUK (Radiation and nuclear safety authority) (1999) 1-75.

[60] D. H. Hur, Y. S. Park, Effect of solution temperature on the pitting behavior and passive film characteristics of alloy 600 in chloride solution. Corrosion 62 (2006) 745-750.

[61] C. O. A. Olsson, D. Landolt, Passive films on stainless steels-chemistry, structure and growth. Electrochimica Acta 48 (2003) 1093-1104.

[62] E. A. Abd El Meguid, A. A. Abd El Latif, Critical pitting temperature for Type 254 SMO stainless steel in chloride solutions. Corrosion Science 49 (2007) 263-275.

[63] G. Lothongkum, S. Chaikittisilp, A. W. Lothongkum, XPS investigation of surface films on high Cr-Ni Ferritic and austenitic stainless steel. Applied Surface Science 218 (2003) 202-209.

[64] E. Otero Huerta, Corrosión y Degradación de Materiales, Síntesis, (ed.), 1997.

[65] A. Fattah-alhosseini, A. Saatchi, M. A. Golozar, K. Raeissi, The transpassive dissolution mechanism of 316L stainless steel. Electrochimica Acta 54 (2009) 3645-3650.

[66] M. H. Moayed, N. J. Laycock, R. C. Newman, Dependence of the critical pitting temperature on surface roughness. Corrosion Science 45 (2003) 1203-1216.

[67] I. C. Lavos-Valereto, I. Costa, S. Wolynec, The electrochemical behavior of Ti-6Al-7Nb Alloy with and without Plasma-Sprayed Hydroxyapatite Coating in Hank's solution. Journal of Biomedical Materials Research. Applied Biomaterials 63 (2002) 664-670.

[68] Sergio Luiz de Assis, S. Wolynec, I. Costa, Corrosion characterization of titanium alloys by electrochemical techniques. Electrochimica Acta 51 (2006) 1815-1819.

[69] G. T. Burstein, P. C. Pistorius, S. P. Mattin, The nucleation and growth of corrosion pits on stainless steel. Corrosion Science 35 (1993) 57.

[70] D. E. Williams, J. Stewart, P. H. Balkwill, The nucleation, growth and stability of micropits in stainless steel. Corrosion Science 36 (1994) 1213-1235.

[71] G. T. Burstein, S. P. Vines, Repetitive nucleation of corrosion pits on stainless steel and the effects of surface roughness. Journal of Electrochemical Society 148 (2001) B504-16.

[72] G. T. Burstein, C. Liu, Nucleation of corrosion pits in Ringer's solution containing bovine serum. Corrosion Science 49 (2007) 4296-4306.

[73] G. T. Burstein, C. Liu, Depassivation current transients measured between identical twin microelectrodes in open circuit. Corrosion Science 50 (2008) 2-7.

[74] G. T. Burstein, Electrochemistry of pit formation and growth. Electrochemical Society Proceedings 19 (2004) 1-12.

[75] G. T. Burstein, C. Liu, R. M. Souto, S. P. Vines, Origins of pitting corrosion. Corrosion Engineering, Science and Technology 39 (2004) 25-30.

[76] M. Kaneko, H. S. Isaacs, Effects of molybdenum on the pitting of ferritic- and austenitics-stainless steels in bromide and chloride solutions. Corrosion Science 44 (2002) 1825-1834.

[77] E. A. Abd El Meguid, N. A. Mahmoud, Inhibition of Bromide - Pitting Corrosion of Type 904L Stainless Steel. Corrosion 59 (2003) 104-111.

[78] E. A. Abd El Meguid, Pitting Corrosion Behaviour of Type 904L Stainless Steel in Sodium Bromide Solutions. Corrosion 53 (1997) 623-630.

[79] J. A. Sedricks, Corrosion of Stainless Steels, John Wiley & Sons, (ed.), 1996.

[80] G. C. Palit, V. Kain, H. S. Gadiyar, Electrochemical Investigations of Pitting Corrosion in Nitrogen-Bearing Type 316LN Stainless Steel. Corrosion 49 (1993) 977.

[81] N. J. Laycock, R. C. Newman, Temperature dependence of the pitting potential for austenitic stainless steels above the critical pitting temperature. Corrosion Science 40 (1998) 887-902.

[82] N. J. Laycock, M. H. Moayed, R. C. Newman, Metastable Pitting and the Critical Pitting Temperature. Jorunal of the Electrochemical Society 145 (1998) 2622-2628.

[83] I. Betova, M. Bojinov, T. Laitinen, K. Mäkelä, P. Pohjanne, T. Saario, The transpassive dissolution mechanism of highly alloyed stainless steels I. Experimental results and modelling procedure. Corrosion Science 44 (2002) 2675-2697.

[84] J. R. Galvele, Transport Processes and the Mechanism of Pitting of Metals. Journal of the Electrochemical Society 123 (1976) 464-474.

[85] J. Mankowski, Z. Szklarska-Smialowska, Studies on accumulation of chloride ions in pits growing during anodic polarization. Corrosion Science 15 (1975) 493-501.

[86] M. Dornhege, C. Punckt, J. L. Hudson, H. H. Rotermund, Spreading of corrosion on stainless steel. Simultaneous Observation of metastable pits and oxide film. Journal of the Electrochemical Society 154 (2007) C24-C27.

[87] A. S. Mikhailov, J. R. Scully, J. L. Hudson, Nonequilibrium collective phenomena in the onset of pitting corrosion. Surface Science 603 (2009) 1912-1921.

[88] C. Punckt, M. Bolscher, H. H. Rotermund, A. S. Mikhailov, L. Organ, N. Budiansky, J. R. Scully, J. L. Hudson, Sudden Onset of Pitting Corrosion on Stainless Steel as a Critical Phenomenon. Science 305 (2004) 1133-1136.

[89] T. T. Lunt, V. Brusamarello, J. R. Scully, J. L. Hudson, Interactions among Localized Corrosion Sites Investigated with Electrodes Arrays. Electrochemical and Solid-State Letters 3 (2000) 271-274.

[90] B. Wu, J. R. Scully, J. L. Hudson, A. S. Mikhailov, Cooperative Stochastic Behavior in Localized Corrosion. Journal of the Electrochemical Society 144 (1997) 1614.

[91] G. Q. Liu, Z. Y. Zhu, W. Ke, E. H. Han, C. L. Zeng, Corrosion Behavior of Stainless Steels and Nickel-Based Alloys in Acetic Acid Solutions Containing Bromide Ions. Corrosion 57 (2001) 730-738.

[92] I. Milosev, H. H. Strehblow, The behavior of stainless steels in physiological solution containing complexing agent studied by X-ray photoelectron spectroscopy. Journal of Biomedical Materials Research 52 (2000) 404-412.

[93] S. Ramya, T. Anita, H. Shaikh, R. K. Dayal, Laser Raman microscopic studies of passive films formed on type 316LN stainless steels during pitting in chloride solution. Corrosion Science 52 (2010) 2114-2121.

[94] J. H. Wang, C. C. Su, Z. Szklarska-Smialowska, Effects of Cl- concentration and Temperature on Pitting of AISI 304 Stainless Steel. Corrosion 44 (1988) 732-737.

[95] P. E. Manning, D. J. Duquette, The effect of temperature (25°-289°C) on pit initiation in single phase and duplex 304L stainless steels in 100 ppm Cl-solution. Corrosion Science 20 (1980) 597-609.

[96] Junbo Huang, Xinqiang Wu, En-Hou Han, Influence of pH on electrochemical properties of passive films formed on Alloy 690 in high temperature aqueous environments. Corrosion Science 51 (2009) 2976-2982.

[97] A. Neville, T. Hodgkiess, An assessment of the corrosion behaviour of High-Grade alloys in seawater at elevated temperature and under a high velocity impinging flow. Corrosion Science 38 (1996) 927-956.

[98] T. Bellezze, G. Roventi, R. Fratesi, Electrochemical characterization of three corrosion-resistant alloys after processing for heating-element sheating. Electrochimica Acta 49 (2004) 3005-3014.

[99] P. W. Atkins, Physical Chemistry, Oxford University Press, (ed.), 1998.

[100] Rabab M.El-Sherif, Khaled M.Ismail, Waheed A.Badawy, Effect of Zn and Pb as alloying elements on the electrochemical behavior of brass in NaCl solutions. Electrochimica Acta 49 (2004) 5139-5150.

[101] A. J. Bard and L. R. Faulkner, Electrochemical Methods. Fundamentals and Applications, John Wiley & Sons, (ed.), 2001.

[102] G. F. Vander Voort, Metallography: Principles and Practice, ASM International, (ed.), 1999.

[103] American Society for Metals, Metallography and Microstructures, ASM International, (ed.), 1995.

[104] F. Mansfeld, J. V. Kendel, Laboratory studies of galvanic corrosion of aluminium alloys., in: R.Raboian, W.D.France (eds.), Galvanic and Pitting Corrosion-Field and Laboratory Studies, ASTM STP 576, ASTM, 1976, 20-47.

[105] F. T. Cheng, K. H. Lo, H. C. Man, NiTi cladding on stainless steel by TIG surfacing process Part II. Corrosion behavior. Surface and Coatings Technology 172 (2003) 316-321.

Tables captions

Table 1. Materials composition (wt%).

Table 2. OCP values of Alloy 31 and welded Alloy 31 in the 1080 g/l LiBr solution at 75ºC, 100ºC, 125ºC and 150ºC .

Table 3. Galvanic parameters of Alloy 31 and welded Alloy 31 in the 1080 g/l LiBr solution at 75ºC, 100ºC, 125ºC and 150ºC.

Figures captions

Figure 1. Cyclic potentiodynamic curves of Alloy 31 (a) and welded Alloy 31 (b) in a 1080 g/l LiBr solution at 75ºC, 100ºC, 125ºC and 150ºC.

Figure 2. Images of Alloy 31 and welded Alloy 31 in the 1080 g/l LiBr solution after the cyclic tests at 75ºC, 100ºC, 125ºC and 150ºC. These images are mosaics created from images obtained with an optical microscope.

Figure 3. Percentages of the damaged area of the Alloy 31 and the welded Alloy 31 after the cyclic tests in the 1080 g/l LiBr solution at 75ºC, 100ºC, 125ºC and 150ºC.

Figure 4. Images taken with an optical microscope of Alloy 31 and welded Alloy 31 in the 1080 g/l LiBr solution after the cyclic tests at 75ºC, 100ºC, 125ºC and 150ºC.

Figure 5. Corrosion Potentials (a) and Corrosion Current Densities (b) of Alloy 31 and Welded Alloy 31 at 75ºC, 100ºC, 125ºC and 150ºC in the 1080 g/l LiBr solution. Error bars denote the standard deviations of the measured values. Symbols denote the average of at least three measurements.

Figure 6. Pitting potential values (a) and passivation current densities (b) of Alloy 31 and welded Alloy 31 in the 1080 g/l LiBr solution at 75ºC, 100ºC, 125ºC and 150ºC. Error bars denote the standard deviations of the measured values. Symbols denote the average of at least three measurements.

Figure 7. Repassivation Potential (a), passivity region (b) and anodic hysteresis loop (c) of Alloy 31 and welded Alloy 31 in the 1080 g/l LiBr solution at 75ºC, 100ºC, 125ºC and 150ºC. Error bars denote the standard deviations of the measured values. Symbols denote the average of at least three measurements.

Figure 8. Passive ranges obtained from the cyclic potentiodynamic curves of Alloy 31 (a) and welded Alloy 31 (b) in the 1080 g/l LiBr solution at 75ºC, 100ºC, 125ºC and 150ºC.

Figure 9. Arrhenius plots of current densities at different potentials from the cyclic potentiodynamic curves of Alloy 31 (a) and welded Alloy 31 (b) in the 1080 g/l LiBr solution at 75ºC, 100ºC, 125ºC and 150ºC.

Figure 10. SEM image of a) Alloy 31 etched for 120 s in 60% HNO_3 at 140 mA/cm^2 and b) the welded metal etched for 120 s in 15ml HNO_3-5 ml Methanol-85 ml H_2O (using backscattered electrons).

Figure 11. EDX analysis on the welded Alloy 31.

Table 1

Material	UNS	Cr	Ni	Mn	Si	Mo	Cu	Fe	S	P	C	N	Al	Co
Alloy 31	N08031	26.75	31.85	1.50	0.10	6.60	1.21	31.43	0.002	0.017	0.005	0.193	---	---
Filler Metal	N06059	22.65	60.58	0.15	0.03	15.40	---	0.58	0.002	0.003	0.002	---	0.16	0.04

Table 2 (revised)

	OCP ($mV_{Ag/AgCl}$)			
	75°C	**100°C**	**125°C**	**150°C**
Alloy 31	-259±15	-213±23	-81±32	-23±8
Welded Alloy 31	-135±7	-234±10	-202±11	-179±13

Table 3 (revised)

Materials	75 ºC		100 ºC		125 ºC		150 ºC	
	Alloy 31	**Welded Alloy 31**	**Alloy 31**	**Welded Alloy 31**	**Alloy 31**	**Welded Alloy 31**	**Alloy 31**	**Welded Alloy 31**
E_{corr} ($mV_{Ag/AgCl}$)	-739	-711	-728	-685	-618	-660	-575	-651
E_{Couple} ($mV_{Ag/AgCl}$)	**-723**		**-701**		**-626**		**-633**	
E_C-E_A (mV)	*28*		*43*		*42*		*77*	
i_{corr} ($\mu A/cm^2$)	8.7A	4.7C	18.6A	17.38C	46.9C	25.2A	62.2C	133.6A
i_G ($\mu A/cm^2$)	**5.2**		**24.9**		**27.3**		**182.5**	
i_G/i_{corr}	*0.6*		*1.3*		*1.1*		*1.4*	

Figure 1 (revised)

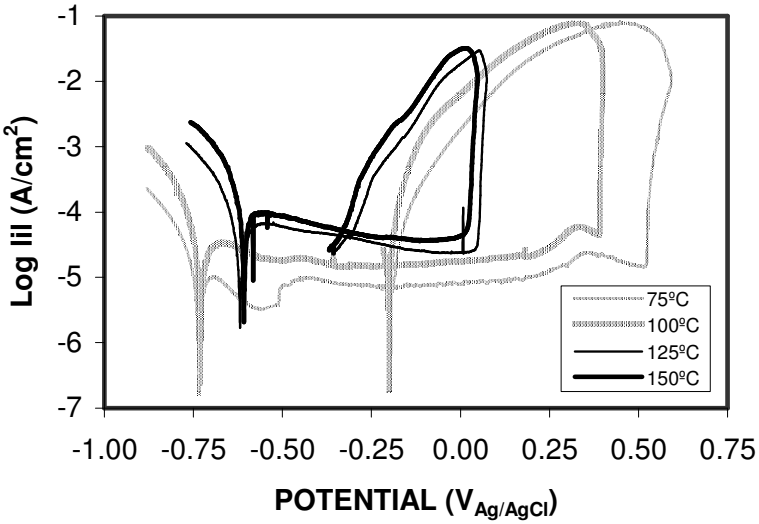

(a)

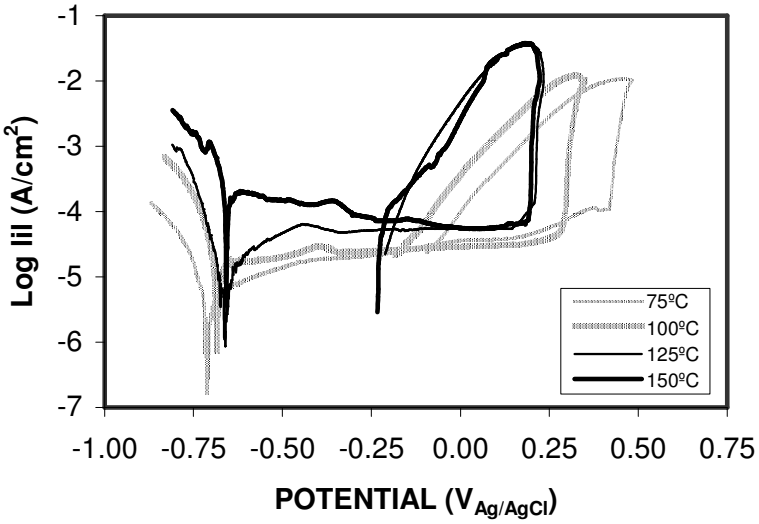

(b)

Figure 2 (revised)

Alloy 31	Welded Alloy 31
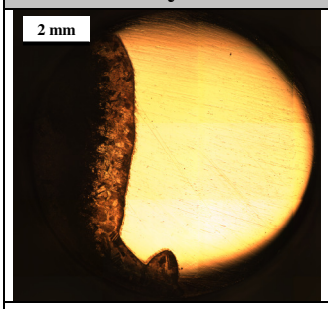	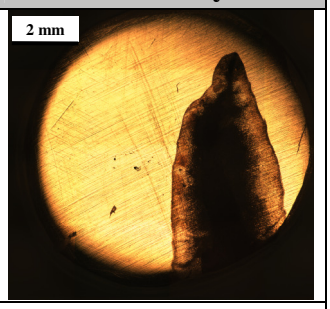
75ºC	75ºC
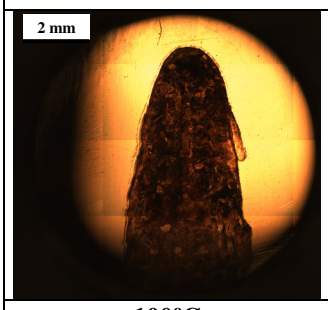	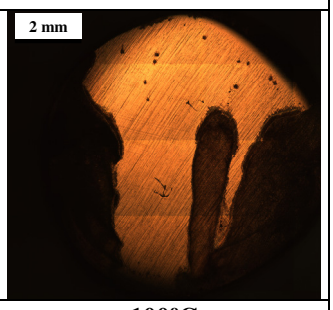
100ºC	100ºC
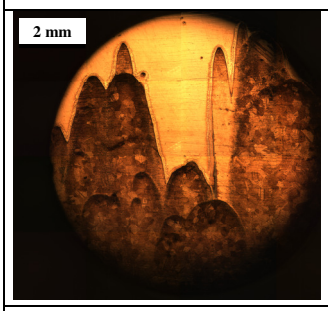	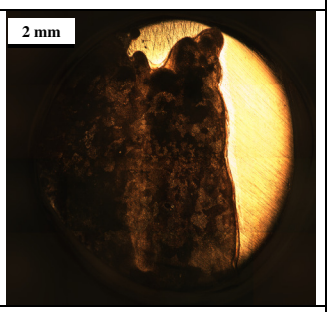
125ºC	125ºC
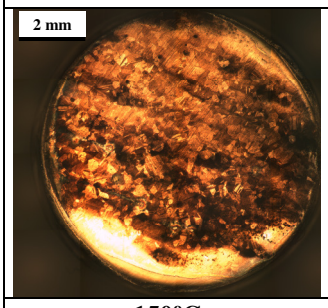	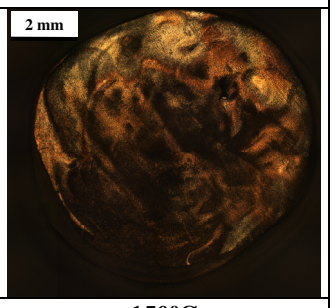
150ºC	150ºC

Figure 3 (revised)

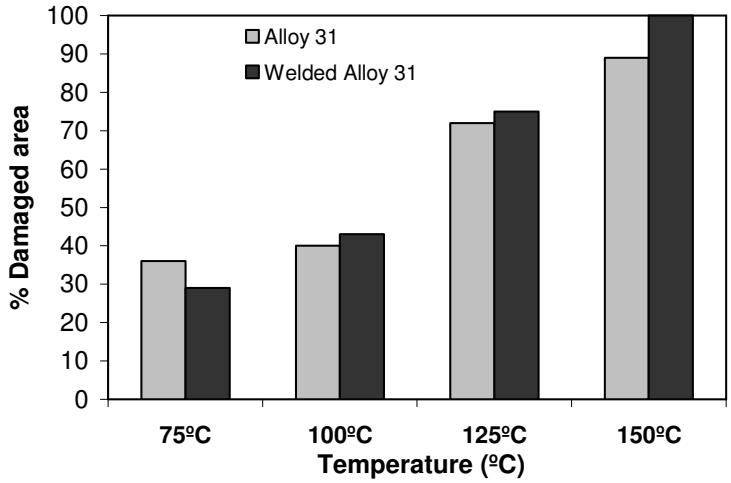

Figure 4 (revised)

Alloy 31	Welded Alloy 31
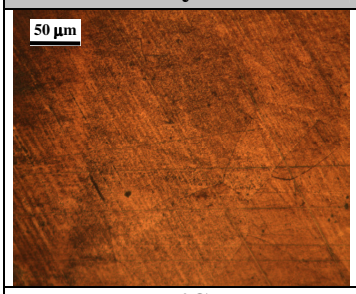	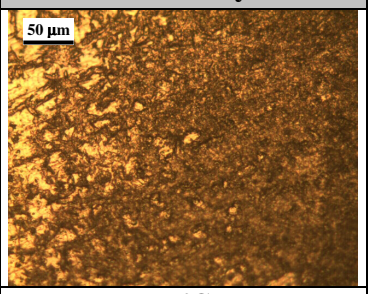
75°C	75°C
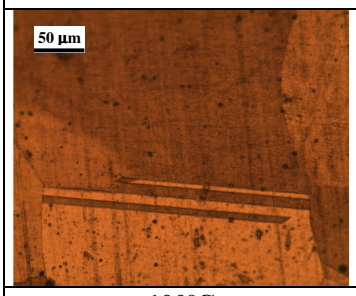	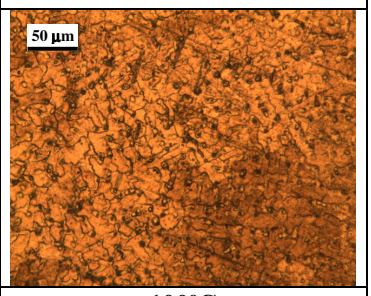
100°C	100°C
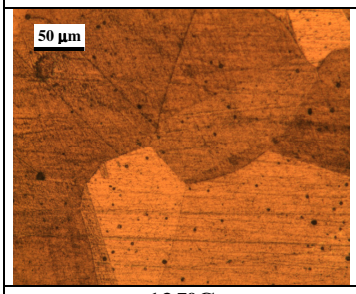	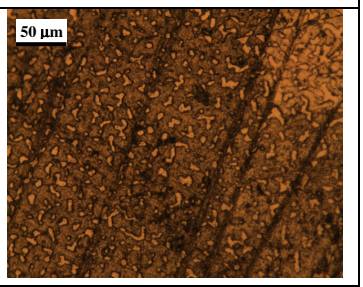
125°C	125°C
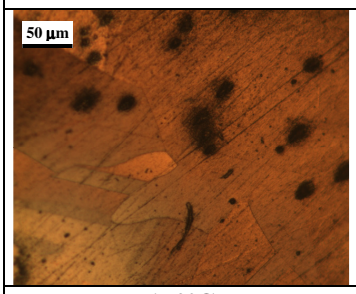	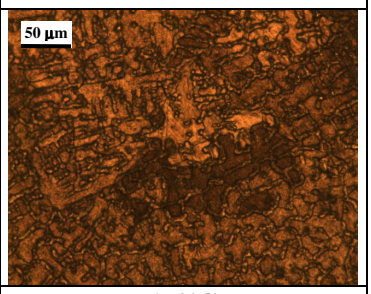
150°C	150°C

Figure 5 (revised)

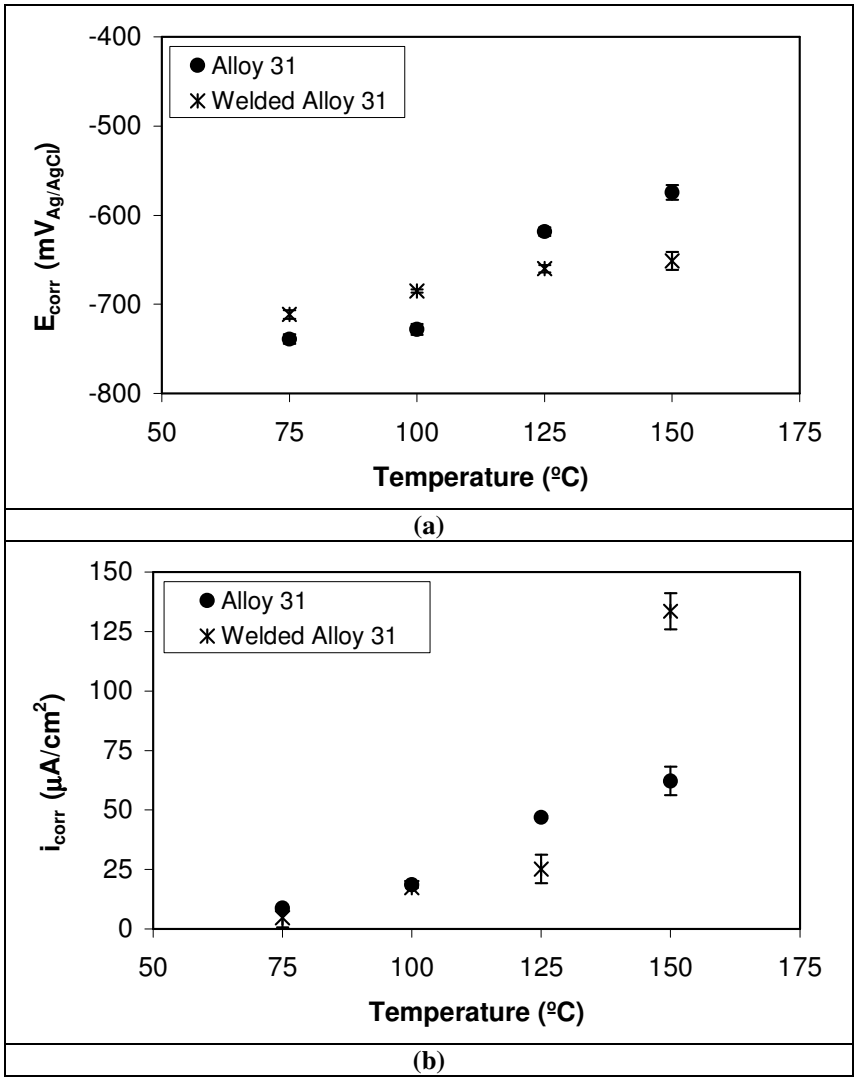

Figure 6 (revised)

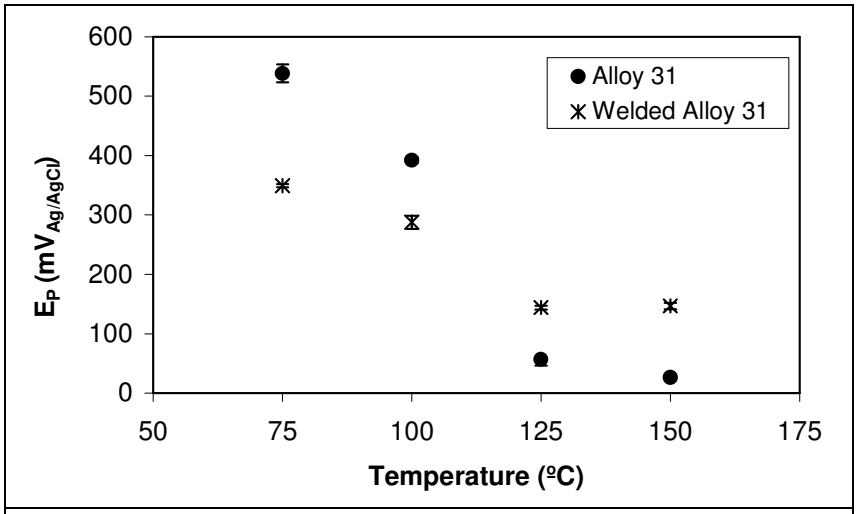

(a)

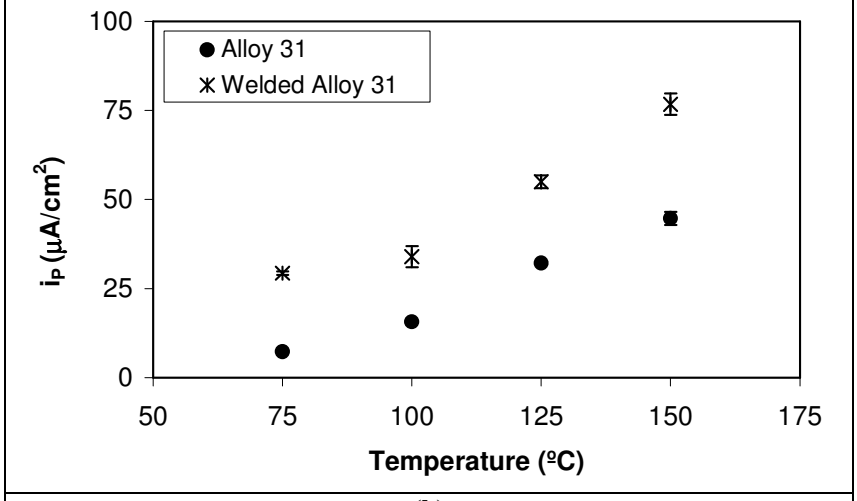

(b)

Figure 7 (revised)

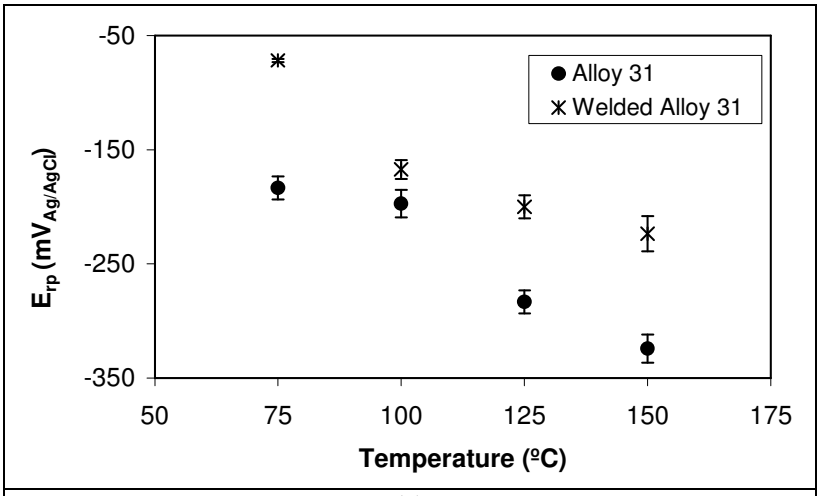

(a)

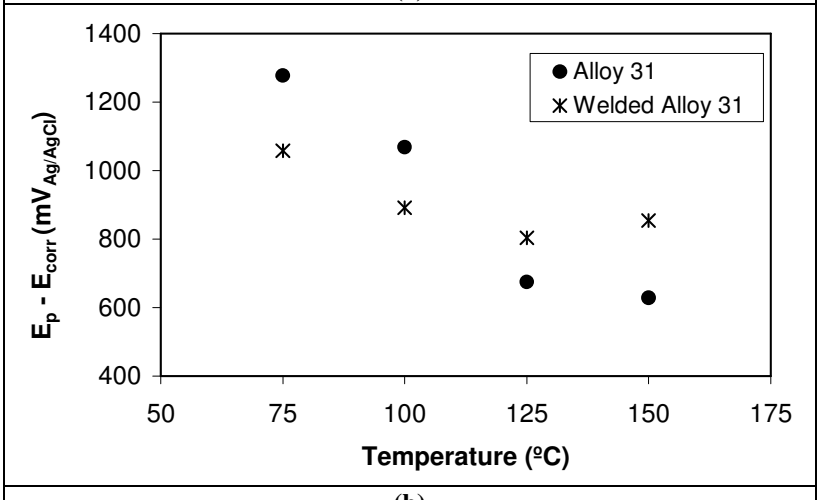

(b)

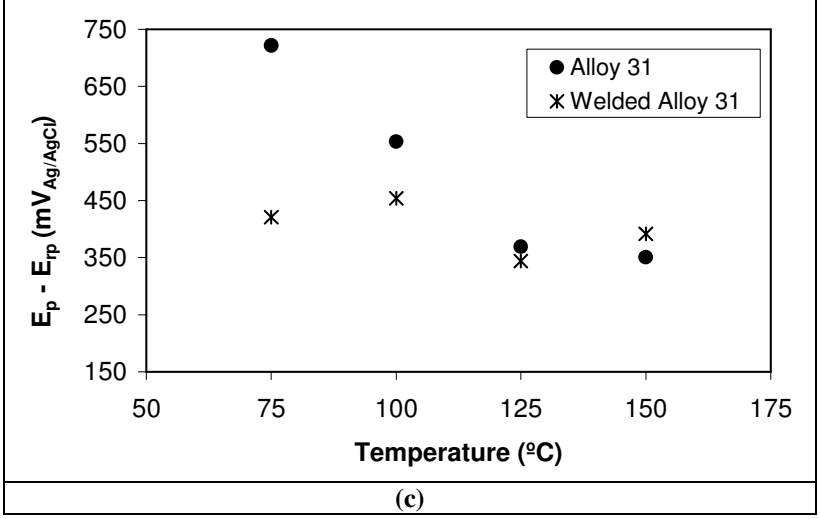

(c)

Figure 8 (revised)

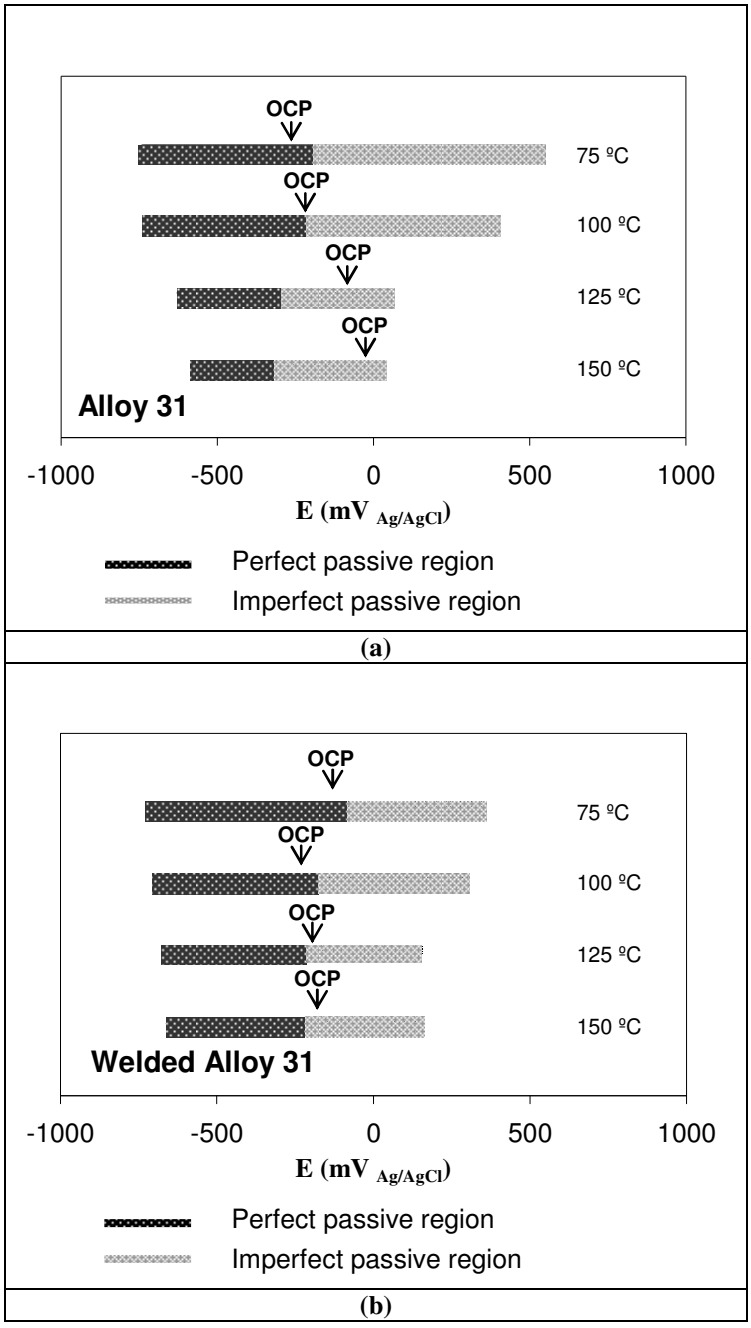

Figure 9 (revised)

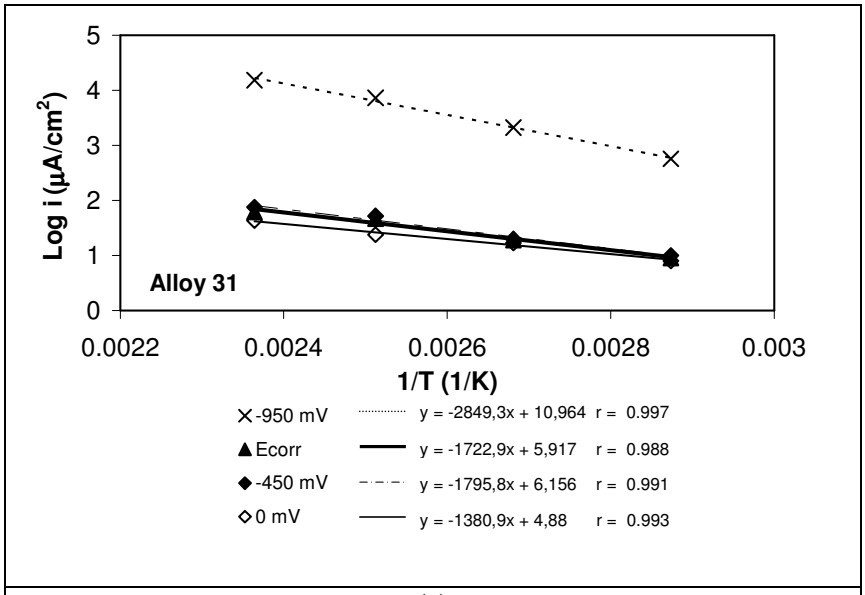

(a)

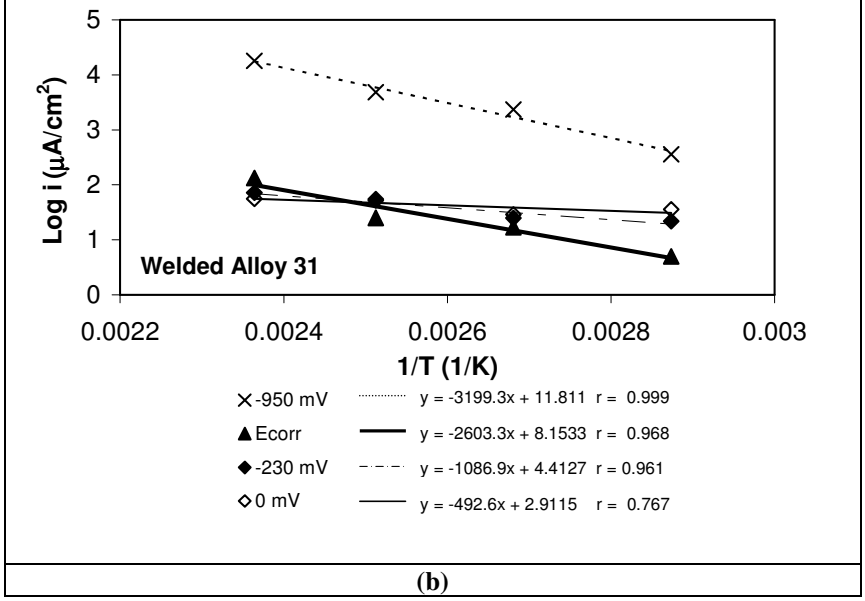

(b)

Figure 10 (revised)

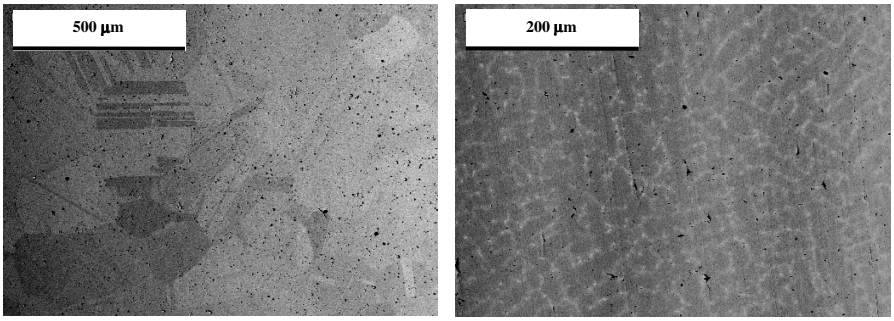

(a) **(b)**

Figure 11 (revised)